Characterization of SLA RNA promoter from dengue virus and its interaction with the viral non-structural NS5 protein

Karl Brillet, Marta Janczuk-Richter, Amanda Poon, Joanne Laukart-Bradley, Eric Ennifar, Isabelle Lebars

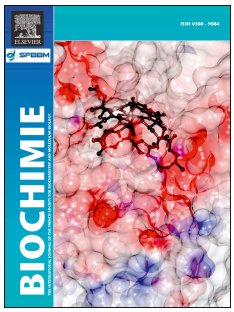

Characterization of SLA RNA promoter from dengue virus and its interaction with the viral non-structural NS5 protein

Karl Brillet, Marta Janczuk-Richter, Amanda Poon, Joanne Laukart-Bradley, Eric Ennifar, Isabelle Lebars

PII: S0300-9084(24)00043-9

DOI: https://doi.org/10.1016/j.biochi.2024.02.005

Reference: BIOCHI 6680

To appear in: *Biochimie*

Received Date: 9 November 2023

Revised Date: 19 February 2024

Accepted Date: 19 February 2024

Please cite this article as: K. Brillet, M. Janczuk-Richter, A. Poon, J. Laukart-Bradley, E. Ennifar, I. Lebars, Characterization of SLA RNA promoter from dengue virus and its interaction with the viral non-structural NS5 protein, *Biochimie* (2024), doi: https://doi.org/10.1016/j.biochi.2024.02.005.

Characterization of SLA RNA promoter from Dengue virus and its interaction with the viral non-structural NS5 protein

Karl Brillet[1], Marta Janczuk-Richter[2], Amanda Poon[2], Joanne Laukart-Bradley[2], Eric Ennifar[1] & Isabelle Lebars[1,*]

[1] Université de Strasbourg, CNRS, Architecture et Réactivité de l'ARN, UPR 9002, F-67000 Strasbourg, France

[2] Creoptix AG (a Malvern Panalytical Brand), CH-8820 Wädenswil, Switzerland.

Shortened Title: The DENV SLA RNA and its interaction with the viral NS5

*To whom correspondence should be addressed:

Dr Isabelle Lebars : i.lebars@ibmc-cnrs.unistra.fr (Tel.: +33 (0) 3 88 41 70 02)

ABSTRACT

The Dengue virus (DENV) is the most significant arthropod-borne viral pathogen in humans with 400 million infections annually. DENV comprises four distinct serotypes (DENV-1 to -4) which complicates vaccine development. Any of the four serotypes can cause clinical illness but with distinctive infection dynamics. Variations in sequences identified within the four genomes induce structural differences in crucial RNA motifs that were suggested to be correlated to the degree of pathogenicity among DENV-1 to -4. In particular, the RNA Stem-loop A (SLA) at the 5'-end of the genome, acts as a key regulator of the viral replication cycle by interacting with the viral NS5 polymerase to initiate the minus-strand viral RNA synthesis and later to methylate and cap the synthesized RNA. The molecular details of this interaction remain not fully described. Here, we report the solution secondary structures of SLA from DENV-1 to -4. Our results highlight that the four SLA exhibit structural and dynamic differences. Secondly, to determine whether SLA RNA contains serotype-specific determinants for the recognition by the viral NS5 protein, we investigated interactions between SLA from DENV -1 to -4 and DENV2 NS5 using combined biophysical approaches. Our results show that NS5 from DENV2 is able to bind SLA from other serotypes, but that other viral or host factors may be necessary to stabilize the complex and promote the catalytically active state of the NS5. By contrast, we show that a serotype-specific binding is driven by specific interactions involving conformational changes within the SLA RNA.

Key Words: DENV, SLA, NS5, structure, interaction

1. INTRODUCTION

1.1 The Dengue Virus

The dengue virus (DENV) is a mosquito-borne virus belonging to the *Flaviviridae* family which also includes the Zika (ZIKV), Yellow fever (YFV), Japanese encephalitis (JEV) and West Nile (WNV) viruses. With 400 million of new infections annually, DENV, considered as one of the most critical viruses, poses a worldwide public health problem with a 30-fold increase in global incidence over the past 50 years. Due to global warming, the DENV mosquito vectors from *Aedes* genus (*Aedes aegypti* and *Aedes albopictus*) are spreading from tropical and sub-tropical regions to more temperate areas, thus expanding the risk of disease [1,2]. Although most infections are asymptomatic or cause mild symptoms (fever, muscle and join pain, nausea, headache and skin rash), in some severe cases, hemorrhagic fever (DHF) and shock syndrome (DSS) occur leading to 22,000 deaths per year. DENV comprises four distinct serotypes (DENV-1 to 4) which complicates vaccine development [3]. Any of the four identified serotypes can produce clinical illness. They share 60 to 70% genetic homology and a similar organization of the virion and the genome [4,5]. The viral genome is a positive-sense single-stranded RNA (ssRNA) virus of 11 kb with 5'- and 3'- untranslated regions (UTR) and a 5' cap. The viral proteins are encoded in a single open reading frame (ORF) which is translated upon infection. The single polypeptide chain is then cleaved by viral and host proteases leading to 3 structural proteins (C, prM, E) and 7 non-structural proteins (NS1, NS2A, NS2B, NS3, NS4A, NS4B and NS5). The majority of antiviral developments targets the non-structural proteins NS3 and NS5 due to their fundamental role in the viral replication cycle [6–9].

1.2 The NS5 viral protein

NS5 is the largest (900 aa) and most conserved protein encoded by *Flaviviruses*, containing two structurally conserved domains linked by a poorly conserved 9 aa sequence among the 4 serotypes: the N-terminal methyltransferase (MTase) domain (263 aa) involved in the 5'-RNA cap synthesis and methylation, and the C-terminal domain which possesses the RNA-dependent RNA polymerase (RdRp) activity. The S-adenosylmethionine (SAM) is used

as the methyl donor by the MTase domain for capping of the nascent genomic RNA [8,9]. Crystal structures of DENV NS5 have been determined [2]. In solution, MTase and RdRp domains are shown to have different relative orientations and the NS5 from DENV-1 to -4 can adopt multiple conformations [10,11]. NS5 binds specifically the RNA stem-loop A (SLA) located in the 5'-UTR to first promote viral RNA synthesis (RdRp function) and later to methylate and cap the synthesized RNA (MTase function) [12–18]. Through its interaction with SLA, NS5 has also been shown to inhibit translation of the viral genome at the initiation stage [19].

1.3 The SLA viral RNA

The 5'-UTR ranges from 95 to 101 nucleotides long, depending on the serotype. The first domain SLA is predicted to adopt a "Y" shape secondary structure in all serotypes with sequence differences in loops and bulges (Fig. 1A) [20,21]. These variations in base composition may influence the degree of the pathogenicity by affecting the three-dimensional structure of the RNA among the serotypes and lead to distinctive infection dynamics [20,22]. Through these studies aiming at correlating RNA structure with pathogenicity, the authors show that the 5'-end of the RNA genome from DENV2, which is associated with more prevalence and severity of the disease, is significantly more rigid than the others [20]. Surprisingly, the reported crystallographic structure of DENV2 SLA shows an L-shaped RNA forming a dimer through intermolecular loop-loop interactions via the side stem-loop (SSL) (Fig. 1B) [23]. By contrast, the solution structure of DENV1 SLA was determined as a monomer adopting a L-shape structure with a folded SSL as described in the predicted secondary structure (Fig. 1C) [24].

1.4 The SLA:NS5 complex

The interaction between SLA and NS5, a key element regulating the replication cycle, is still not fully characterized among the four serotypes. NS5 from one serotype is able to bind SLA from other serotypes, suggesting that the polymerase would recognize the shape of the

RNA [13,14,25]. Studies based on fluorescence experiments showed that the SLA:NS5 complex formation was salt-dependent with a 1:1 stoichiometry of NS5 to SLA [25]. Structural elements of the promoter SLA such as the side stem-loop (SSL), the top loop (TL) and the U bulge were identified as critical structural elements for DENV2 viral replication in infected cells [14]. Previous works based on sequence alignments, phylogenetic analysis and secondary structure predictions show that motifs similar to SLA exists in all *Flavivirus* genomes [20,21,26–28] suggesting a common mechanism regulating the viral replication among this family. The conserved Motif F located in the RdRp domain in the NS5 protein has been suggested to bind SLA prior to viral RNA replication and therefore controlling the relative orientation of the two domains to promote the active state of the protein [29]. Recently, a cryo-EM structure of an SLA bound to the DENV3 NS5 revealed specific interactions between the Top Loop of SLA and the basic “thumb pocket” of the RdRp domain on the one hand, and the bottom stem of SLA and the MTase domain on the other hand [30].

In this work, we first report the solution secondary structure of SLA from DENV-1 to -4 as determined by Nuclear Magnetic Resonance (NMR). We show that the four RNAs exhibit different structural and dynamic behaviours. Secondly, to determine whether SLA-RNA contains serotype-specific determinants for the recognition by the NS5 polymerase, we investigated the *in vitro* SLA interaction from DENV-1 to -4 with the NS5 from DENV2 by using Electrophoretic Mobility Shift Assay (EMSA), Isothermal Titration Calorimetry (ITC), Grating-Coupled Interferometry (GCI) and NMR. Our study focused on DENV2 NS5:SLA recognition provides evidence for a binding process based on specific interactions inducing structural rearrangement within the RNA in the case of a serotype-specific interaction. By contrast, we show that DENV2 NS5 is able to recognize non-serotype-specific SLA but that other factors may be needed in that case to stabilize the complex and promote the catalytically active state of the NS5.

2. MATERIALS AND METHODS

2.1 RNA sample preparation

Milligram quantities of SLA RNA were prepared unlabeled and uniformly $^{13}C/^{15}N$ by *in vitro* transcription from oligonucleotide templates using in-house T7 RNA polymerase [31]. A sequence modification (U-A to G-C) was designed at the 5'-end to obtain a better transcription yield (Fig. 1A). The DNA templates were purchased from IDT (Belgium). Labeled NTPs (nucleotides triphosphate) were purchased from Eurisotop (UK). Transcription conditions were optimized with varying magnesium concentrations in 25 μL reaction mixtures in 40 mM TRIS-HCl pH 8, 1 mM spermidine, 0.01% Triton X-100, 5 mM dithiothreitol (DTT) and 10% polyethylene glycol (PEG 8000), in the presence of 4 mM of each NTP [31,32]. Preparative *in vitro* transcriptions were next performed with 19.2 mM $MgCl_2$ for DENV-1 and -2 SLA, and 16 mM $MgCl_2$ for DENV-3 and -4 SLA in 5 to 7 mL reaction volumes. The reaction mixture was incubated at 37°C during 4.5 h. After phenol extraction and ethanol precipitation, RNAs were next purified on 8 M urea denaturing polyacrylamide gels followed by electroelution [32]. After ethanol precipitation, RNAs were dialyzed against water. Samples were next dried using a SpeedVac and resuspended at a chosen concentration in buffers used for ITC and UV melting experiments. For NMR studies, RNA samples were dialyzed against the buffer used for NMR. Each sample was refolded by heating at 95°C (2 min) and snap-cooled at 4°C. The concentrations of RNA samples were determined on a Nanodrop Spectrometer using molar extinction coefficients.

2.2 Expression and purification of NS5 polymerase

Full-length DENV2 NS5 was cloned in a pET-28a(+)-TEV vector (GenScript). The protein was expressed in *Escherichia coli* BL21 (DE3) cells. The cells were grown overnight at 37°C in Luria broth (LB) medium containing 30 $\mu g.mL^{-1}$ kanamycin. Next, 2 L of a 2*LB medium supplemented with the same antibiotic were inoculated at 0.04 OD_{600}. The cells were grown at

37°C to an OD_{600} of 0.7. The expression of the NS5 protein was induced by addition of 1 mM isopropyl-β-D-1-thiogalactopyranoside (IPTG). The temperature was next lowered to 20°C. The induced culture was incubated at 20°C for 3 hours. Cells were pelleted and lysed by sonication in a lysis buffer (50 mM TRIS pH 7.5, 400 mM KCl, 20 mM Imidazole, 1 mM DTT) supplemented with 0.25 $mg.mL^{-1}$ Lysozyme and a protease cocktail inhibitor (Thermo scientific). After centrifugation, His-tagged proteins were isolated by affinity chromatography on a HisTrap HP column (GE Healthcare). NS5 was eluted with an imidazole gradient of 20 to 500 mM in the elution buffer (50 mM TRIS pH 7.5, 400 mM KCl, 1 mM DTT). The fractions containing NS5 were collected. The pooled fractions mixed with in-house TEV protease (1:10 w/w ratio) were dialyzed overnight at 4°C against the elution buffer. After dialysis, the sample was loaded onto the HisTrap HP column equilibrated with the elution buffer supplemented with 20 mM imidazole. Fractions containing the cleaved NS5 were concentrated by using a centrifugal filter device (MWCO 50 kDa, Amicon Ultra from Merck Millipore) and further purified by size exclusion chromatography using a Superdex 200 Increase 10/300 (GE Healthcare) equilibrated with 50 mM sodium phosphate pH 7.4, 400 mM KCl and 1 mM DTT. The purity of the protein was >95% (estimated by SDS-PAGE and Mass Spectrometry). The concentration of NS5 was spectrophotometrically determined with an extinction coefficient (ε_{280}) of 217260 $cm^{-1}.M^{-1}$.

2.3 UV melting experiments

Thermal denaturation of SLA RNAs was monitored on a CARY3500 UV/vis spectrophotometer (Agilent) equipped with an 8-position sample holder and a Peltier temperature control accessory. The experiments were performed at 1 μM in 50 mM sodium phosphate buffer, at pH 6.4 at 20°C, in 100 μL micro quartz cuvettes. The RNAs were refolded as described above and the magnesium was next added at concentrations ranging from 0.1 to 6.0 mM. A cuvette that contained the buffer with no magnesium was used as a reference. Samples were overlaid with 100 μL of mineral oil to prevent evaporation at high temperature. An initial 15 minute

equilibrium time at 25°C was included prior to the temperature ramping. Denaturation of the samples was achieved by increasing the temperature at 1°C.min^{-1} from 25 to 95°C and followed at 260 nm. The melting temperature (*Tm*) was determined as the maximum of the first derivative of the UV melting curves. Each experiment was repeated independently two or three times.

2.4 Electrophoretic Mobility Shift Assay experiments

Experiments were performed in the presence and in the absence of S-Adenosylhomocystein (SAH). 1 μM of RNA (SLA from DENV-1 to -4 and a 57-nt RNA control) was incubated with increasing amount of NS5 or NS5:SAH 1:1 (1 to 10 μM) in 10 μL of the binding buffer (20 mM TRIS pH 7.5, 150 mM KCl, 2 mM $MgCl_2$, 5% glycerol and 1 mM DTT) for 15 min on ice. 2 μL of 6X bromophenol blue dye (0.25% bromophenol blue and 30% glycerol) was added next. Reactions were loaded onto a 1% agarose gel in 1X Tris/Borate/EDTA (TBE) buffer migrated at 100 V for 40 min at 4°C. Bands were visualized after ethidium bromide staining by GelDoc Imaging System (BIO-RAD).

2.5 Isothermal Titration Calorimetry experiments

ITC experiments were performed using a PEAQ-ITC microcalorimeter (Malvern Panalytical). RNA sample was refolded by heating at 95°C (2 min) and snap-cooled at 4°C (5 min) in the buffer used for ITC experiments. The concentration of RNA sample in the syringe and protein in the cell were 550 μM and 58 μM, respectively. Titration experiments were performed at 5°C in 50 mM sodium phosphate buffer pH 6.4 supplemented with 300 mM KCl and 1 mM DTT, under constant stirring at 750 rpm, with 19 x 2 μL injections into 205 μL sample cell volume, with 3 min between injections. Each experiment was accompanied by the corresponding control experiment in which the RNA at the same concentration was injected into the buffer alone. Buffer corrected ITC profiles were then analyzed using MicroCal PEAQ-ITC analysis software (Malvern Panalytical).

2.6 Grating Coupled Interferometry

GCI experiments were performed with the Creoptix WAVEdelta system (Malvern Panalytical). Interactions between the protein and RNA constructs were measured using a PCP-NTA WAVEchip (quasi-planar polycarboxylate hydrogel with pre-immobilized NTA). The Chip was conditioning with 0.1 M borate pH 9, 1 M NaCl and 0.25 M EDTA pH 8 buffer. After standard activation with 0.5 mM $NiCl_2$ (420 s) and with a 1:1 mix of 400 mM *N*-[3-(dimethylamino)propyl]-*N′*-ethylcarbodiimide hydrochloride (EDC) and 50 mM *N*-hydroxysuccinimide (NHS) (Xantec) (420 s), the His-Tagged NS5 protein (30 $\mu g.mL^{-1}$ in running buffer: 50 mM sodium phosphate pH 6.4, 150 mM KCl and 1 mM DTT) was captured on channel 1, resulting in an immobilization mass of approximatively 6500 $pg.mm^{-2}$. Final surface passivation was performed with 1 M ethanolamine, pH 8 along with 0.35 M EDTA conditioning for 420 s. Channel 2 was only activated and passivated as described above and was used as reference. A flow rate of 10 $\mu L.min^{-1}$ was used during all the steps of chip surface preparation.

Binding experiments were performed at 15°C in 50 mM sodium phosphate (pH 6.4) containing 150 mM KCl and 1 mM DTT. The waveRAPID® method was used for kinetic measurements which use pulses of analyte at increasing duration from a single concentration [33]. RNA concentrations were used at 13.3, 15.2, 13.4, 10.0 and 11.4 μM for SLA-D1, -D2, -D3, -D4 and the control, respectively. RNAs were injected over the surface at a flow rate of 50 $\mu L.min^{-1}$ per channel with an association time of 25 s followed by a dissociation time of 200 s. The apparent concentration of the analytes in the sensing area over the 6 injection pulses was calibrated with a pulsed injection of running buffer supplemented with 0.5% DMSO, using the same injection parameters as for the analytes.

Data were analyzed using the Creoptix WAVEcontrol 4.5.17 evaluation software. The data were fitted using the 1:1 binding model. Empty channel and blanked injections were used for double referencing.

2.7 NMR experiments

NMR experiments were recorded at 700 MHz on an Avance III Bruker spectrometer equipped with a z-gradient TCI cryoprobe. NMR data were processed using TopSpin (Bruker) and analyzed with NMRFAM-SPARKY software packages [34].

Free unlabeled and labeled RNA samples volumes were 150 µL in 3 mm NMR tubes at concentrations ranging from 0.2 to 0.4 mM. NMR experiments were performed in 50 mM sodium phosphate buffer at pH 6.4 in 90/10 H_2O/D_2O. NMR data were acquired at 6°C, 10°C, 15°C, 20°C, 25°C, 30°C and 37°C for exchangeable protons. Solvent suppression was achieved using combined “Jump and Return” and WATERGATE sequences [35–37]. Two-dimensional NOESY spectra in 90/10 H_2O/D_2O were acquired with mixing time of 50 ms, 70 ms, 150 ms, 300 ms and 400 ms at 6°C, 10°C, 15°C and 20°C. Base-pairing was established via sequential nuclear Overhauser effects (nOes) observed in 2D NOESY spectra at different mixing times. ^{1}H-^{15}N HSQC experiments were acquired at 10°C, 15°C and 30°C. ^{1}H-^{13}C HSQC experiments were measured at 15°C and 30°C in 90/10 H_2O/D_2O. ^{13}C and/or ^{15}N decoupling during acquisition was achieved using the GARP composite pulse sequence.

NS5 was concentrated by using a centrifugal filter device and the buffer was subsequently exchange against 50 mM sodium phosphate at pH 6.4, 300 mM KCl and 1 mM DTT. RNA:NS5 complexes were formed first by successive addition of the protein to the RNA by monitoring imino protons at 15°C. Saturation of RNAs was observed at a 1:1 stoichiometry. SLA:NS5 complexes were next concentrated by using centrifugal filter devices and the buffer was subsequently exchanged against 50 mM sodium phosphate, 100 mM KCl and 1 mM DTT. Sample volumes were 150 to 180 µL in 3 mm NMR tubes. One-dimensional NMR spectra, 2D ^{1}H-^{15}N HSQC and 2D ^{1}H-^{13}C HSQC experiments were then recorded. Magnesium was finally added at a concentration of 1, 2 and 3 mM.

3. RESULTS AND DISCUSSION

3.1 Variability of the SLA secondary structures dynamic among DENV-1 to -4 serotypes

3.1.1 NMR solution secondary structures of SLA from DENV-1 to -4

The NMR structural studies were performed on SLA constructs which sizes vary from 61-nt to 63-nt according to the serotype (Fig. 1A). Secondary structures were characterized by the analysis of 2D NOESY recorded in 90/10 H_2O/D_2O at various temperatures. Imino protons are observable between 9 and 15 ppm provided that they are protected from exchange *i.e.,* involved in hydrogen bonds. All imino protons were assigned via sequential nuclear Overhauser effects (NOEs) observed in 2D NOESY (Fig. 2B). Briefly, the A:U Watson-Crick base-pairs are discriminated from G:C base-pair by the strong correlation between the U-H3 imino proton and the A-H2 proton at short mixing time. In a G:C base-pair, two strong NOEs between the G-H1 and the cytosine amino protons are observable. Next, sequential assignments were based on NOE cross-peaks observable between protons of neighboring base-pair, using U-H3 as a starting point. In addition, the four SLA share common regions which were used to help and confirm assignments.

The assignment of DENV1 SLA (SLA-D1) is depicted in the Supplementary Figure 1. The solution secondary structure of SLA-D1 is close to the predicted structure with additional non canonical base-pairs A21•G32, G12•A49 and U5•U57 while the predicted Watson-Crick A24:U29 and A39:U48 are not formed (Fig. 1A and 2A). The SSL forms a CUUG loop as supported by characteristic chemical shifts of G45-H1, G41-H1 and U43-H3 at 13.25 ppm, 12.62 ppm and 11.60 ppm respectively, and NOEs pattern [38,39]. In the recent structure published by Sun and Varani [40], A21•G32 and U5•U57 base pairs are also observable but G12•A49 is not formed and A39:U48 is visible. It is worth noting that in their study the CUUG loop in the SSL and the apical loop (A24 to U29) have been replaced by GNRA and UUCG tetraloops respectively, which can explain the differences observed (Fig. 1C).

Imino protons of SLA from DENV2 (SLA-D2) were unambiguously assigned and confirmed by analysis of ^{1}H-^{15}N HSQC (Supplementary Fig. 2). The assignment of S1 and S2 stems was similar to SLA-D1. Sequential NOEs connectivities support the existence of a monomeric RNA as a major form comprising the predicted S1, S2 and S3 stems with the three additional base pairs U5•U58, G17•A36 and G12•A50 as described in the crystallographic structure published by Lee and co-workers [23]. The major monomeric form was confirmed by native gel electrophoresis (Supplementary Fig. 3). In contrast to the predicted structure, the SSL adopts two distinct conformations in solution as illustrated by imino-imino sequential NOEs from U43 to U48 (Supplementary Fig. 2). In the a-form, U43:G46 forms a stable U:G pair as shown by the characteristic strong NOE correlation and stacked on G41:C46, suggesting that the C42 may be looped out. By contrast, in the b-form, weaker NOE cross-peaks are observable between G46-H1 and U43-H3 and with G41-H1, indicative of a more flexible structure compared to the a-form. This suggests that the C42 could be stacked between G41 and U43 in the b-form inducing a destabilization of the hydrogen bond network (Fig. 2A). The solution structure of the SSL differs from the crystal structure in which G41 to C47 residues are involved in an intermolecular loop-loop complex leading to a SLA-SLA dimer (Fig. 1B), with G13 and A14 base-paired with C49 and U48, respectively (Fig. 2A). In a study of the structure of the DENV2 genomic RNA based on SHAPE analysis in virion and ex virion, slight differences are also observed in the SSL [41]. This underlines the ability of the SSL to adopt different local structures while the rest of the RNA is highly structured. In addition, we observe a major monomeric SLA RNA at concentration below 0.5 mM with a minor alternative conformation (indicated by stars in Fig. 2B). We cannot exclude that it could correspond to the dimeric SLA, a conformation that would have been favored in the crystal.

In SLA from DENV3 (SLA-D3), G:U wobble base-pairs predicted in stem S1 were easily identified from the very strong NOE between the G-H1 and the U-H3 at short mixing time (50 ms, (Supplementary Fig. 4). Stems S1 and S2 are formed as predicted. However, the upper part of SLA-D3 adopts two major distinct conformations with a co-existing minor conformation which has not been determined. The first one (a-form) differs from the prediction with the

formation of two helical segments and no SSL. The second conformation (b-form) contains an additional A22•G33 pair and the SSL capped with the CUUG tetraloop is formed, while the central stem (C16-G39 to A19-U36) is not observed (Fig. 2). Our results show that this RNA is able to adopt several flexible conformations with only Stems S1 and S2 being rigid. These observations highlight its particular behaviour compared to other serotypes in the same condition.

The strategy of assignment of SLA from DENV4 (SLA-D4) was similar to SLA-D2 and SLA-D1 (Supplementary Fig. 5). SLA-D4 adopts one conformation close to the predicted structure, with A25:U30 and A40:U49 not being observed.

Our NMR results show that SLA from serotypes 1, 2 and 4 adopt “Y-shape” secondary structures in solution with little variations compared to the predicted structures, whilst the SLA-D3 has two major conformations with a common bottom stem. However, we cannot exclude that all SLA could adopt other conformations not detectable by NMR.

3.1.2 Stability of SLA-D1 to -4 structures and impact of salts

UV melting experiments were carried out to examine the thermal stability of the four SLA in the buffer used for NMR (Fig. 3A). A slight global variation of the melting temperature (*Tm*) is observed among the four serotypes. The derivative of UV melting curves of SLA-D2 displays two distinct major transitions around 50°C and smallest transition above 55°C (Fig. 3A). SLA-D1, -D3 and -D4 exhibit similar derivative curves profiles: large transitions with shoulders corresponding to distinct and close *Tm* in the same range as SLA-D2 (ΔTm < 5°C, Fig. 3A) with SLA-D3 showing the lowest *Tm* value, followed by SLA-D1. We next examined the impact of magnesium ions on the stability of the four RNAs. A clear increase of *Tm* is observed upon increasing magnesium concentrations, indicating an enhancement in the thermal stability of the RNA as expected. SLA-D1 to -D4 display similar *Tm* values while the lowest value is observed for SLA-D3 (Supplementary Fig. 6). Notably, at the highest magnesium concentration (6 mM), three clear *Tm* are observable for SLA-D2 being the most stable.

In addition to UV melting experiments, we used NMR to finely analyze the denaturation of RNA constructs. NMR spectra recorded from 15°C to 37°C show differences in terms of stability for SLA-D1 to -D4 (Fig. 3B). Imino protons are observable provided that they are involved in H-bond. With increasing temperature, the resonance broadening or disappearing indicates that the region becomes flexible or single-stranded, respectively. As shown in Figure 3B, SLA-D3 is the most flexible among the 4 serotypes. At 37°C, four base-pairs are melted in the lower helix of the a-form while in the b-form, the upper part becomes unfolded with only stems S1 and S2 maintained. In the case of SLA-D1, six base-pairs located at stem-loop junctions are destabilized at 37°C. The SSL from SLA-D4 is destabilized as well as A19:U36 and U5•U57 base-pairs. The SLA-D2 is the most rigid with its structure fully maintained at 37°C. Our studies provide evidences that SLA from the four serotypes exhibit differences in terms of stability and that they can be classified as follows from the most rigid to the most flexible: SLA-D2 > SLA-D4 > SLA-D1 > SLA-D3.

3.2 The NS5 and SLA interaction

3.2.1 The binding of NS5 from DENV2 induces structural changes within SLA-D2

We first focused on the interaction between NS5 and SLA from DENV-2, which is often associated with the severe form of the disease. We examined the interaction between the RNA and the protein using EMSA experiments. As the bottom stem of SLA has been shown to interact with NS5 near its MTase active site containing the SAM [23,30], experiments were performed in the presence and in the absence of SAH, the by-product of the methylation reaction with SAM in order to analyze the potential effect on RNA binding. The NS5 polymerase binds the RNA inducing a band shift variation that increased with increasing amount of the protein (1 to 10 μM), similarly with and without SAH (Fig. 4A). The same experiment performed with control RNAs shows that no interaction is detected in such conditions (Fig. 6A). We next used ITC microcalorimetry to characterize the SLA-D2 binding to NS5. The measurement at 150 mM KCl as for EMSA experiments, was not amenable due to the precipitation of the protein

at the high concentration required for the experiment (> 50 μM). However, the dissociation constant (K_D) was calculated at 8.4 ± 1.4 μM in the presence of 300 mM KCl, a salt concentration well-suited for protein stability at high concentration (Fig. 4B). ITC data show that the binding is an endothermic entropy-driven event indicative of the release of water molecules from the binding region into the solvent. Next, the use of GCI technology by the waveRAPID® kinetic method allowed accurate measurements at 150 mM KCl with the protein at low concentration (0.3 μM) captured onto the surface of the chip and RNA used as analytes. GCI data yield K_D calculated at 5.4 ± 0.6 μM (Table 1), in line with ITC data obtained in similar conditions, while no binding was observed with the negative control RNA (Fig. 4C) [33]. It is worth noting that our results cannot be compared directly to previous studies based on fluorescence experiments in completely different conditions (buffer, pH, salt) and with the DENV3 NS5 and uncapped SLA-DENV2/3 for which the K_D measurement varied from 0.1 to 0.5 μM [23,25]. We cannot also exclude that the affinity may be enhanced in the presence 5'-cap which have been shown to interact with the MTase domain of NS5 [30].

NMR was then used to map the interaction between the RNA and the NS5 protein. The chemical shift of imino protons were monitored as a function of the NS5 concentration to identify the RNA helical regions in contact with the NS5 protein (Fig. 5A). One-dimensional ^{1}H and 2D ^{1}H-^{15}N HSQC spectra were recorded. NS5 binds the RNA at a 1:1 stoichiometry which is in agreement with previous and recent works studying the interaction between the DENV3 NS5 and SLA from DENV2 or -4 [25,30]. The addition of the protein to SLA-D2 resulted in several changes. G23, G27, U29, U30, U58 and all imino protons located in the SSL disappeared upon binding to NS5, highlighting modifications of solvent accessibility which can be interpreted as conformational changes such as a melting of these regions (Fig. 5A and 5B). U5 at 11.18 ppm showed a significant chemical shift variation (0.11 ppm). Beside these effects, other imino protons were almost not affected by the addition of the protein. Conformational changes of SLA upon NS5 binding were further investigated using non-exchangeable protons from adenines (see Supplementary Fig. 7 for assignment). C2H2 chemical shift perturbations

upon NS5 binding were monitored using 2D ^{1}H-^{13}C HSQC (Fig. 5C). Upon NS5 binding, A24, A40, A_{SSL1}, A_{SSL2} and A_{TL} disappeared or broadened while A36 and A50 were slightly shifted. In contrast, adenines located in stems S1 and S2 remained almost unaffected. Finally, no supplementary effect on the complex was observed upon the addition of magnesium (Fig. 5A). Our NMR data show that the NS5 polymerase from DENV2 targets specifically the U5•U58/U57 tri-bulge and the Top Loop of SLA-D2 and unwinds the SSL and the upper part of Stem S3 (Fig. 5D), which is consistent with previous studies. In fact, Lodeiro *et al.* [14] demonstrated that mutations shortening the SSL or impairing the base-pairing resulted in a delayed viral replication while a complete deletion of the SSL abolished the replication. Mutations in the Top Loop and in the U tri-bulge also induced a decreased or a delayed viral replication. Later, a model of a NS5:SLA complex based on the crystallographic structure of DENV2 SLA suggested that the Top Loop is positioned towards the basic binding pocket of the RdRp domain and that the 5'-terminus of SLA binds the protein near the active site of the MTase domain, with the SSL unwinded pointing outward [23]. Recently, a cryo-EM structure of a complex between DENV3 NS5 and DENV4 SLA shows that the Top Loop is bound to the basic thumb pocket of the RdRp domain and that the bottom stem interacts with the MTase domain where the 5'-RNA cap lies into the MTase catalytic pocket [30]. The DENV4 SLA adopts a V-shaped structure in the complex with the SSL outward but folded, contrasting with the model proposed for the DENV2 NS5:SLA complex [23]. This suggests that the conformation adopted in the complex by SLA from each serotype may originate from its intrinsic rigidity or flexibility. In fact, the stem 3 (S3) in DENV2 SLA contains 6 base pairs (bp), an A-bulge followed by 3 bp, while DENV4 SLA S3 is formed by 2 bp, 2 internal bulges followed by 4 bp (Fig. 2A), leading to differences in their flexibility and the co-axial stacking of helices. In the case of DENV2 SLA, which S3 has been suggesting to play a critical role in NS5 binding due to its high rigidity [20], the constraint on the bending of the RNA upon NS5 binding would promote the unwinding of the SSL. The DENV4 SLA with its S3 more flexible may not undergo the same constraint upon NS5 binding, consequently maintaining the SSL folded. Finally, in our studies, although we used a shorter RNA construct without the capped 5'-

tetraribonucleotide, the NS5 protein binds the U5-U57/U58 bulge with the structure of the stem maintained. The alteration of the structure of the four base-pairs downstream the tri-bulge was shown to affect replication [12]. In the cryo-EM structure, one U-bulge is in the proximity of the helix 3 of the MTase domain. Interestingly, this U-bulge has been found fully conserved during the species evolution [21]. All this suggests that the U-bulge would serve as anchor for protein binding, even in the absence of the 5'-cap provided that a minimum of downstream base pairs is present.

3.2.2 The NS5 from DENV2 is able to bind SLA from other serotypes through a different mechanism

To determine whether SLA-RNA contains serotype-specific determinants for the recognition by the NS5 polymerase, we investigated the *in vitro* SLA interaction from DENV-1, -3 and -4 with the NS5 from DENV2. We first examined the interaction between the RNA and the protein using EMSA experiments as described in section 3.1.1. The NS5 binds the RNA inducing a band shift variation with increasing amount of the protein, similarly with and without SAH, with an apparent K_D in the micromolar range as observed for SLA-D2 (Fig. 6B to 6D). We next used the GCI technology with the waveRAPID® kinetic method to determine more accurately the affinity between the RNA variants and NS5. Dissociation constants (K_D) were estimated at 11.3 ± 2.8 μM, 11.2 ± 2.6 μM and 5.7 ± 0.5 μM for SLA-D1, -D3 and -D4, respectively (Fig. 7). DENV2 NS5 binds SLA-D4 with a K_D similar to SLA-D2 while slightly lower affinities are observed for SLA-D1 and -D3. The dissociation rate constants (k_d) values for these two RNAs are 1.3- and 1.5-fold higher than for SLA-D2, whereas the association rate constants (k_a) are reduced by 1.6- and 1.4-fold respectively (Table 1).

Finally, to further investigate the mechanism of binding, NMR experiments were performed on complexes formed between each SLA RNA and the protein at a 1:1 stoichiometry. The imino protons were used to map the interaction between the RNA and the NS5 protein (Fig. 7). With SLA-D1 and -D3, the addition of the protein induced a uniform broadening of all resonances which is characteristic of a non-specific binding. The complexation of the NS5 to SLA-D4

induced also a global broadening, but to a lesser extent, concomitant with the disappearance of U48/U36 and U58, and little chemical shift variations. As observed with SLA-D2, the protein contacts the conserved U-bulge previously identified as critical for recognition and the SSL. However, in contrast to SLA-D2, the SSL is not melted, G42, U44 and G46 still being observable.

Our results underline how changes in structure and flexibility may result in different subtle mechanisms of recognition. We show that the DENV2 NS5 is able to interact with all DENV SLA but with different mechanisms. In fact, a non-specific binding is observed with SLA-D1 and -D3. In the case of SLA-D4, the NS5 targets the Top Loop and the U-bulge without the dissolution of SSL structure, by contrast to SLA-D2. With SLA-D2 and SLA-D4 identified as the most rigid structures among the four serotypes, our results suggest first that the particular identified rigidity of DENV2 SLA may be an important factor for DENV2 NS5 recognition, which is in agreement with studies demonstrating its structural requirement for the virus replication [14]. Secondly, the same authors observed that the DENV2 NS5 was able to recognize *in vitro* and *in vivo* DENV1 SLA as well as DENV2 SLA, in a context of a 160-nt RNA template and a cDNA in which the SLA were swapped. The structure of SLB stem-loop located in the 5' UTR downstream the SLA was found not essential for viral replication [15]. However, the 5' UAR sequence embedded into the SLB motif is complementary to the 3' UAR sequence located in the 3'UTR region, which allows the cyclization of the viral genome (Fig. 8), therefore promoting the minus-strand RNA synthesis [12]. Lodeiro *et al.* showed that the length of the spacer between the SLA and the 5' UAR sequence, out of the context of the structure of the SLB, influences the efficiency of the polymerase activity [14]. DENV3 NS5 has been shown to bind *in vitro* both DENV3 and DENV2 SLA, but with a slightly higher affinity for DENV2 [25]. This work also pointed out that DENV3 NS5 recognizes DENV3 SLA itself as well as an SLA construct encompassing the additional 10-nt spacer at its 3'-end. In our studies focused on SLA, the lack of the spacer and the 5' UAR could explain the differences of NS5 binding to other serotypes. This suggests that the DENV2 NS5 can recognize a non-serotype-specific

SLA but that other factor or RNA regions are needed to stabilize the complex and may contribute to the polymerase function.

4. CONCLUSIVE REMARKS

The structure of RNA is fundamental for many viral functions, as found in HCV, HIV, coronaviruses, ZIKV, DENV and other viruses. Several studies aiming at deciphering the variability among the four serotypes of DENV suggested that significant differences in sequence similarity may modulate RNA structures which could be correlated to the degree of pathogenicity of each serotype [20,22]. In particular, the SLA structure located at the 5'-end of the genomic RNA, was found to adopt in DENV2 a distinct secondary structure from other serotypes with a more rigid and longer S3 stem. These observed differences may affect the binding of the NS5 polymerase and therefore the replication cycle and the virulence of strains. DENV1 is the most widespread while DENV2 is associated with severe cases of the disease. In this work, we report the solution secondary structures of DENV-1 to -4 SLA showing that the four RNAs exhibit *in vitro* different structural and dynamic behaviours, SLA-D2 being the most rigid and SLA-D3, the most flexible. This study highlights intrinsic properties of SLA characteristic of each serotype. However, the SLA "Y-shaped" secondary structural features have been shown to be highly conserved among *Flaviviruses* and essential to complete the SLA function in the replication cycle [21]. This raises the question if other factors would help to maintain the SLA conserved architecture to fulfill its role in particular in the case of flexible structure.

To determine whether SLA-RNA contains serotype-specific elements for the recognition by the NS5, we investigated the *in vitro* SLA interaction from DENV-1, -2, -3 and -4 with the NS5 from DENV2. Our study focused on DENV2 NS5:SLA recognition provides evidence for a binding process based on specific interactions in the case of a serotype-specific interaction: the NS5 targets the Top Loop and the U-bulge and unwinds the SSL structure. By contrast, we show that DENV2 NS5 is able to recognize SLA from other serotypes but that other viral and host factors may be needed in that case to stabilize the complex and promote the catalytically active state of the NS5. The mechanisms behind DENV NS5 recognition of SLA and its complete description will require further investigations. If other regions of the RNA or other factors activate the NS5:SLA complex is still an open question. Our present results however suggest

that serotype-specific elements would favor a stable NS5:SLA complex and therefore its activity.

SUPPLEMENTAL MATERIALS

Supplemental material is available for this article.

ACKNOWLEDGEMENTS

This work benefited from access to the Liquid NMR Service at IGBMC Instruct Centre FR1 (Strasbourg, France), an Instruct-ERIC centre. Financial support was provided by Instruct-ERIC (PID 12415, PID 17683). This work benefited from GCI experiments performed at Creoptix AG (Switzerland). This work was supported by the Centre National de la Recherche Scientifique (CNRS) and the “Agence Nationale de la Recherche” (ANR, grant DeZincRNA ANR-21-CE12-0024).

We thank Katia Zanier for providing the plasmid for TEV protease expression and purification. We thank the Cortecs Scientific Facilities and the MBioFaSt platform of the University of Strasbourg.

Author Contributions

Conceptualization of the project and design of the experiments, I.L.; RNA samples preparation, I.L.; NS5 expression and purification, K.B. and I.L.; TEV expression and purification, K.B. and I.L.; UV melting experiments and analysis, I.L.; NMR experiments, I.L.; NMR spectra assignments, I.L.; EMSA experiments, I.L.; ITC design, experiments, and analysis, K.B. and E.E.; GCI design, experiments, and analysis, M.J.-R., A.P. and J.L.-B.; writing-original draft preparation, I.L.; writing-review and editing, K.B., E.E., I.L., J.L.-B., M.J.-R., and A.P. All authors have read and agreed to the published version of the manuscript.

REFERENCES

[1] A. El Sahili, J. Lescar, Dengue Virus Non-Structural Protein 5, Viruses 9 (2017) 91. https://doi.org/10.3390/v9040091.
[2] A. El Sahili, T.S. Soh, J. Schiltz, A. Gharbi-Ayachi, C.C. Seh, P.-Y. Shi, S.P. Lim, J. Lescar, NS5 from Dengue Virus Serotype 2 Can Adopt a Conformation Analogous to That of Its Zika Virus and Japanese Encephalitis Virus Homologues, Journal of Virology 94 (2019). https://doi.org/10.1128/JVI.01294-19.
[3] J.O. Obi, H. Gutiérrez-Barbosa, J.V. Chua, D.J. Deredge, Current Trends and Limitations in Dengue Antiviral Research, TropicalMed 6 (2021) 180. https://doi.org/10.3390/tropicalmed6040180.
[4] J. Blok, Genetic Relationships of the Dengue Virus Serotypes, Journal of General Virology 66 (1985) 1323–1325. https://doi.org/10.1099/0022-1317-66-6-1323.
[5] E.M. Kellman, D.K. Offerdahl, W. Melik, M.E. Bloom, Viral Determinants of Virulence in Tick-Borne Flaviviruses, Viruses 10 (2018) 329. https://doi.org/10.3390/v10060329.
[6] S. Apte-Sengupta, D. Sirohi, R.J. Kuhn, Coupling of replication and assembly in flaviviruses, Current Opinion in Virology 9 (2014) 134–142. https://doi.org/10.1016/j.coviro.2014.09.020.
[7] D. Luo, S.G. Vasudevan, J. Lescar, The flavivirus NS2B–NS3 protease–helicase as a target for antiviral drug development, Antiviral Research 118 (2015) 148–158. https://doi.org/10.1016/j.antiviral.2015.03.014.
[8] Y. Zhao, T.S. Soh, S.P. Lim, K.Y. Chung, K. Swaminathan, S.G. Vasudevan, P.-Y. Shi, J. Lescar, D. Luo, Molecular basis for specific viral RNA recognition and 2′-O-ribose methylation by the dengue virus nonstructural protein 5 (NS5), Proc. Natl. Acad. Sci. U.S.A. 112 (2015) 14834–14839. https://doi.org/10.1073/pnas.1514978112.
[9] M. Issur, B.J. Geiss, I. Bougie, F. Picard-Jean, S. Despins, J. Mayette, S.E. Hobdey, M. Bisaillon, The flavivirus NS5 protein is a true RNA guanylyltransferase that catalyzes a two-step reaction to form the RNA cap structure, RNA 15 (2009) 2340–2350. https://doi.org/10.1261/rna.1609709.
[10] C. Bussetta, K.H. Choi, Dengue Virus Nonstructural Protein 5 Adopts Multiple Conformations in Solution, Biochemistry 51 (2012) 5921–5931. https://doi.org/10.1021/bi300406n.
[11] W.G. Saw, G. Tria, A. Grüber, M.S. Subramanian Manimekalai, Y. Zhao, A. Chandramohan, G. Srinivasan Anand, T. Matsui, T.M. Weiss, S.G. Vasudevan, G. Grüber, Structural insight and flexible features of NS5 proteins from all four serotypes of Dengue virus in solution, Acta Crystallogr D Biol Crystallogr 71 (2015) 2309–2327. https://doi.org/10.1107/S1399004715017721.
[12] C.V. Filomatori, A 5' RNA element promotes dengue virus RNA synthesis on a circular genome, Genes & Development 20 (2006) 2238–2249. https://doi.org/10.1101/gad.1444206.
[13] L. Yu, M. Nomaguchi, R. Padmanabhan, L. Markoff, Specific requirements for elements of the 5′ and 3′ terminal regions in flavivirus RNA synthesis and viral replication, Virology 374 (2008) 170–185. https://doi.org/10.1016/j.virol.2007.12.035.
[14] M.F. Lodeiro, C.V. Filomatori, A.V. Gamarnik, Structural and Functional Studies of the Promoter Element for Dengue Virus RNA Replication, Journal of Virology 83 (2009) 993–1008. https://doi.org/10.1128/JVI.01647-08.
[15] D.E. Alvarez, M.F. Lodeiro, S.J. Ludueña, L.I. Pietrasanta, A.V. Gamarnik, Long-Range RNA-RNA Interactions Circularize the Dengue Virus Genome, Journal of Virology 79 (2005) 6631–6643. https://doi.org/10.1128/JVI.79.11.6631-6643.2005.
[16] C. Polacek, J.E. Foley, E. Harris, Conformational Changes in the Solution Structure of the Dengue Virus 5′ End in the Presence and Absence of the 3′ Untranslated Region, Journal of Virology 83 (2009) 1161–1166. https://doi.org/10.1128/JVI.01362-08.
[17] L. Liu, H. Dong, H. Chen, J. Zhang, H. Ling, Z. Li, P.-Y. Shi, H. Li, Flavivirus RNA cap methyltransferase: structure, function, and inhibition, Front Biol (Beijing) 5 (2010) 286–303. https://doi.org/10.1007/s11515-010-0660-y.
[18] D. Ray, A. Shah, M. Tilgner, Y. Guo, Y. Zhao, H. Dong, T.S. Deas, Y. Zhou, H. Li, P.-

Y. Shi, West Nile virus 5'-cap structure is formed by sequential guanine N-7 and ribose 2'-O methylations by nonstructural protein 5, J Virol 80 (2006) 8362–8370. https://doi.org/10.1128/JVI.00814-06.
[19] T. Fajardo, T.J. Sanford, H.V. Mears, A. Jasper, S. Storrie, D.S. Mansur, T.R. Sweeney, The flavivirus polymerase NS5 regulates translation of viral genomic RNA, Nucleic Acids Research 48 (2020) 5081–5093. https://doi.org/10.1093/nar/gkaa242.
[20] B. Mishra, A. Balaji, H. Beesetti, S. Swaminathan, R. Aduri, The RNA secondary structural variation in the cyclization elements of the dengue genome and the possible implications in pathogenicity, Virusdisease 31 (2020) 299–307. https://doi.org/10.1007/s13337-020-00615-w.
[21] B. Samanta, Structural evolution of SLA promoter in mosquito-borne flaviviruses: A sequence-structure based phylogenetic framework, Virology 562 (2021) 110–120. https://doi.org/10.1016/j.virol.2021.07.007.
[22] R. Delli Ponti, M. Mutwil, Structural landscape of the complete genomes of dengue virus serotypes and other viral hemorrhagic fevers, BMC Genomics 22 (2021) 352. https://doi.org/10.1186/s12864-021-07638-7.
[23] E. Lee, P.J. Bujalowski, T. Teramoto, K. Gottipati, S.D. Scott, R. Padmanabhan, K.H. Choi, Structures of flavivirus RNA promoters suggest two binding modes with NS5 polymerase, Nat Commun 12 (2021) 2530. https://doi.org/10.1038/s41467-021-22846-1.
[24] Y.-T. Sun, G. Varani, Structure of the dengue virus RNA promoter, RNA 28 (2022) 1210–1223. https://doi.org/10.1261/rna.079197.122.
[25] P.J. Bujalowski, W. Bujalowski, K.H. Choi, Interactions between the Dengue Virus Polymerase NS5 and Stem-Loop A, Journal of Virology 91 (2017). https://doi.org/10.1128/JVI.00047-17.
[26] M.A. Brinton, J.H. Dispoto, Sequence and secondary structure analysis of the 5′-terminal region of flavivirus genome RNA, Virology 162 (1988) 290–299. https://doi.org/10.1016/0042-6822(88)90468-0.
[27] T.S. Gritsun, E.A. Gould, Origin and evolution of flavivirus 5′UTRs and panhandles: Trans-terminal duplications?, Virology 366 (2007) 8–15. https://doi.org/10.1016/j.virol.2007.04.011.
[28] P. Leyssen, N. Charlier, P. Lemey, F. Billoir, A.-M. Vandamme, E. De Clercq, X. De Lamballerie, J. Neyts, Complete Genome Sequence, Taxonomic Assignment, and Comparative Analysis of the Untranslated Regions of the Modoc Virus, a Flavivirus with No Known Vector, Virology 293 (2002) 125–140. https://doi.org/10.1006/viro.2001.1241.
[29] U. Potapova, S. Feranchuk, G. Leonova, S. Belikov, The rearrangement of motif F in the flavivirus RNA-directed RNA polymerase, International Journal of Biological Macromolecules 108 (2018) 990–998. https://doi.org/10.1016/j.ijbiomac.2017.11.009.
[30] T. Osawa, M. Aoki, H. Ehara, S. Sekine, Structures of dengue virus RNA replicase complexes, Molecular Cell (2023) S1097276523004707. https://doi.org/10.1016/j.molcel.2023.06.023.
[31] J.F. Milligan, O.C. Uhlenbeck, Synthesis of small RNAs using T7 RNA polymerase, Meth. Enzymol. 180 (1989) 51–62.
[32] J.R. Wyatt, M. Chastain, J.D. Puglisi, Synthesis and purification of large amounts of RNA oligonucleotides, BioTechniques 11 (1991) 764–769.
[33] Ö. Kartal, F. Andres, M.P. Lai, R. Nehme, K. Cottier, waveRAPID—A Robust Assay for High-Throughput Kinetic Screens with the Creoptix WAVEsystem, SLAS Discovery 26 (2021) 995–1003. https://doi.org/10.1177/24725552211013827.
[34] W. Lee, M. Tonelli, J.L. Markley, NMRFAM-SPARKY: enhanced software for biomolecular NMR spectroscopy, Bioinformatics 31 (2015) 1325–1327. https://doi.org/10.1093/bioinformatics/btu830.
[35] M. Piotto, V. Saudek, V. Sklenár, Gradient-tailored excitation for single-quantum NMR spectroscopy of aqueous solutions, J. Biomol. NMR 2 (1992) 661–665.
[36] V. Sklenar, M. Piotto, R. Leppik, V. Saudek, Gradient-Tailored Water Suppression for 1H-15N HSQC Experiments Optimized to Retain Full Sensitivity, Journal of Magnetic Resonance, Series A 102 (1993) 241–245. https://doi.org/10.1006/jmra.1993.1098.

[37] P. Plateau, M. Gueron, Exchangeable proton NMR without base-line distorsion, using new strong-pulse sequences, Journal of the American Chemical Society 104 (1982) 7310–7311. https://doi.org/10.1021/ja00389a067.
[38] F.M. Jucker, A. Pardi, Solution Structure of the CUUG Hairpin Loop: A Novel RNA Tetraloop Motif, Biochemistry 34 (1995) 14416–14427. https://doi.org/10.1021/bi00044a019.
[39] A. Oxenfarth, F. Kümmerer, S. Bottaro, R. Schnieders, G. Pinter, H.R.A. Jonker, B. Fürtig, C. Richter, M. Blackledge, K. Lindorff-Larsen, H. Schwalbe, Integrated NMR/Molecular Dynamics Determination of the Ensemble Conformation of a Thermodynamically Stable CUUG RNA Tetraloop, J. Am. Chem. Soc. (2023) jacs.3c03578. https://doi.org/10.1021/jacs.3c03578.
[40] Y.-T. Sun, G. Varani, Structure of the Dengue Virus RNA Promoter, Biochemistry, 2022. https://doi.org/10.1101/2022.04.15.488410.
[41] E.A. Dethoff, M.A. Boerneke, N.S. Gokhale, B.M. Muhire, D.P. Martin, M.T. Sacco, M.J. McFadden, J.B. Weinstein, W.B. Messer, S.M. Horner, K.M. Weeks, Pervasive tertiary structure in the dengue virus RNA genome, Proceedings of the National Academy of Sciences 115 (2018) 11513–11518. https://doi.org/10.1073/pnas.1716689115.
[42] M. Zuker, Mfold web server for nucleic acid folding and hybridization prediction, Nucleic Acids Research 31 (2003) 3406–3415. https://doi.org/10.1093/nar/gkg595.
[43] K. Brillet, D. Martinez-Zapien, G. Bec, E. Ennifar, A.-C. Dock-Bregeon, I. Lebars, Different views of the dynamic landscape covered by the 5'-hairpin of the 7SK small nuclear RNA, RNA 26 (2020) 1184–1197. https://doi.org/10.1261/rna.074955.120.
[44] D.A. Wassarman, J.A. Steitz, Structural analyses of the 7SK ribonucleoprotein (RNP), the most abundant human small RNP of unknown function, Mol. Cell. Biol. 11 (1991) 3432–3445. https://doi.org/10.1128/mcb.11.7.3432.

TABLES

Table 1. Kinetic parameters and Dissociation constants (determined by GCI at 15°C) of the interaction between DENV2 NS5 and SLA from serotypes 1 to 4.

RNA	k_a (10^4 $M^{-1}.s^{-1}$)	k_d (10^{-1} s^{-1})	K_D (μM)
SLA-D2	2.09 ± 0.15	1.12 ± 0.04	5.4 ± 0.6
SLA-D1	1.29 ± 0.26	1.45 ± 0.07	11.3 ± 2.8
SLA-D3	1.48 ± 0.27	1.66 ± 0.07	11.2 ± 2.6
SLA-D4	2.42 ± 0.16	1.39 ± 0.03	5.7 ± 0.5

FIGURE LEGENDS

Figure 1. (A) Predicted SLA secondary structures of SLA from DENV serotypes 1 to 4 by using the Mfold Web server [42]. Sequence variations compared to DENV2 SLA are indicated in bold and nucleotides that have altered for transcription purpose are shown as an outline. **(B)** View of the DENV2 SLA structure solved by Crystallography [23]. The loop-loop interaction via the Side Stem Loop is depicted. **(C)** View of the DENV1 SLA structure as determined by NMR [24].

Figure 2. NMR secondary structures of SLA RNA from serotype 1 to 4. **(A)** NMR solution secondary structures of DENV -1 to -4 SLA. The SSL in SLA-D2 adopts two forms in equilibrium for which strong and weak NOEs are indicated with large and thin black lines, respectively. The SLA-D3 adopts two distinct major conformations. Base-pairs that are melted with increasing temperature are indicated in cyan. A and C residues that are not involved in Watson-Crick base-pairs and G and U that are not hydrogen bonded are colored in dark blue. Black color indicates that residues remain visible with increasing temperature. **(B)** Imino protons region of 1D NMR spectra recorded for SLA-D1, -D2, -D3 and -D4, at 15°C in 50 mM sodium phosphate buffer at pH 6.4. All imino protons were assigned via sequential NOEs observed in 2D-NOESY experiments. Tentative assignments are indicated in italics. Stars indicate the presence of a minor form. In the case of DENV2 and DENV3, the two conformations “a” and “b” are indicated in red and blue, respectively.

Figure 3. Stability of the SLA RNA from serotypes 1 to 4. **(A)** Left: UV melting curves at 260 nm absorbance in the absence of magnesium for SLA-D1 (blue), -D2 (light blue), -D3 (grey) and -D4 (green). Right: Derivative of UV melting curves at 260 nm for SLA-D1 (blue), -D2 (light blue), -D3 (grey) and -D4 (green). **(B)** Imino protons region of 1D NMR spectra recorded for SLA-D1, -D2, -D3 and -D4, at 15°C and 37°C in 50 mM sodium phosphate buffer at pH 6.4.

Residues that undergo broadening with increasing temperature are indicated in cyan. “a” and “b” letters indicate the two forms identified for DENV2 and -3.

Figure 4. Interaction between DENV2 NS5 and SLA-D2. **(A)** EMSA showing the interaction between the NS5 polymerase and SLA RNA from DENV2 in the absence of SAH (top) and in the presence of SAH (bottom). The RNA (1 μM) was titrated with increasing concentrations of NS5 and NS5:SAH at a 1:1 ratio from 1 to 10 μM. **(B)** ITC thermogram for the binding of SLA-D2 to NS5 at 5°C in 50 mM sodium phosphate at pH 6.4 with 300 mM KCl and 1 mM DTT. The top panel shows power versus time trace, and the bottom panel shows integrated heat value as a function of [RNA]/[NS5] ratio. Data were fitted using the single-site binding model. **(C)** Kinetic curves of the SLA (top) and the control RNA (bottom) binding to NS5 obtained by the waveRAPID® method at 15°C in 50 mM sodium phosphate at pH 6.4 with 150 mM KCl and 1 mM DTT. The red curves are the measuring signals and the black ones, the fitting curves. Data were fitted using the 1:1 binding model. The control RNA corresponds to the 5’ terminal hairpin of the 7SK RNA (57 nt) which structure has been solved by NMR and Crystallography [43].

Figure 5. Mapping of the Interaction between DENV2 NS5 and SLA using NMR. **(A)** Spectra for free SLA (top) and for NS5:SLA complex at 1:1 ratio, recorded at 15°C in the presence of 1 mM Mg^{2+}. Broken lines indicate imino protons that undergo chemical shifts variations and broadening. **(B)** Overlay of ^{1}H-^{15}N HSQC spectra recorded at 15°C showing H1-N1 and H3-N3 of the free RNA (black) and the RNA in complex with NS5 at a ratio of 1:1 (blue). In the free RNA, the two conformations of the SSL are indicated in blue and red. **(C)** Overlay of ^{1}H-^{13}C HSQC spectra recorded at 15°C showing H2-C2 of the free RNA (black) and the RNA in complex with NS5 at a ratio of 1:1 (blue). In the free RNA, the two conformations of the SSL are indicated in blue and red. Tentative assignments are indicated in italic. A_{SSL1} and A_{SSL2} could be either A44 or A45 in the a-form (red) and in the b-form (blue) as these two adenines could not be distinguished. A_{TL} refers to adenines in the Top Loop. **(D)** Secondary structures of the free SLA (left) and the bound SLA (right). The cyan color indicates residues which imino

protons are shifted or disappeared upon binding. Adenine residues that undergo variations upon binding are indicated in dark blue.

Figure 6. Interaction between DENV2 NS5 and RNA. EMSA are shown for two control RNA **(A)**, SLA-D1 **(B),** SLA-D3 **(C)**, and SLA-D4 **(D)**, in the absence and in the presence of SAH. RNA (1 µM) were titrated with increasing concentrations of NS5 and NS5:SAH from 1 to 10 µM. The bromophenol blue and the xylene cyanol are indicated with "BB" and "XC", respectively. The first control RNA (right) corresponds to the 5' terminal hairpin of the 7SK RNA (57 nt) which structure has been solved by NMR and Crystallography [43]. The second control (left) corresponds to a longer version of this RNA (the first domain of 7SK RNA) which size is 108 nt. Its secondary structure has been determined by Wasserman and Steitz [44]. Experiments with the two control RNA in the presence of SAH led to the same results (data not shown).

Figure 7. Interaction of NS5 from DENV2 with non-serotype-specific RNA. Kinetic curves obtained by the waveRAPID® method (left panels) and NMR Titrations (right panels) for RNA binding to NS5 are shown for SLA-D1 **(A)**, SLA-D3 **(B)** and SLA-D4 **(C)**. For SLA-D3 **(B)**, assignments of the two forms "a" and "b" are indicated in red and blue respectively. Experiments were recorded at 15°C. The GCI measured and fitted kinetic curves are shown in red and black, respectively. Imino protons region of 1D NMR spectra recorded at 15°C for free RNA (top) and bound RNAs (bottom) are shown for SLA-D1, -D3 and -D4. The stars indicate resonances arising from the protein.

Figure 8. Schematic representation of the DENV genome structures. The equilibrium between "linear" and "circular" forms is depicted. The viral genome with a 5'-cap contains 5'- and 3'-untranslated regions (UTR) and a single open reading frame (ORF) which is translated into 3 structural (light blue) and 7 non-structural proteins (dark blue). The secondary structures of the 5'-UTR is shown: the stem-loop A (SLA), the stem-loop B (SLB) and the capsid region hairpin

(cHP). The 3'-UTR contains 3 domains: the domain I (variable region), the domain II (dumbbell structures) and the domain III (conserved sequence CS, a short stem-loop sHP and the 3'-SL). The 5'-3' complementary regions involved in the cyclization of the genome are indicated: 5'UAR and 3'UAR are indicated in cyan, and 5'CS and 3'CS are indicated with red boxes.

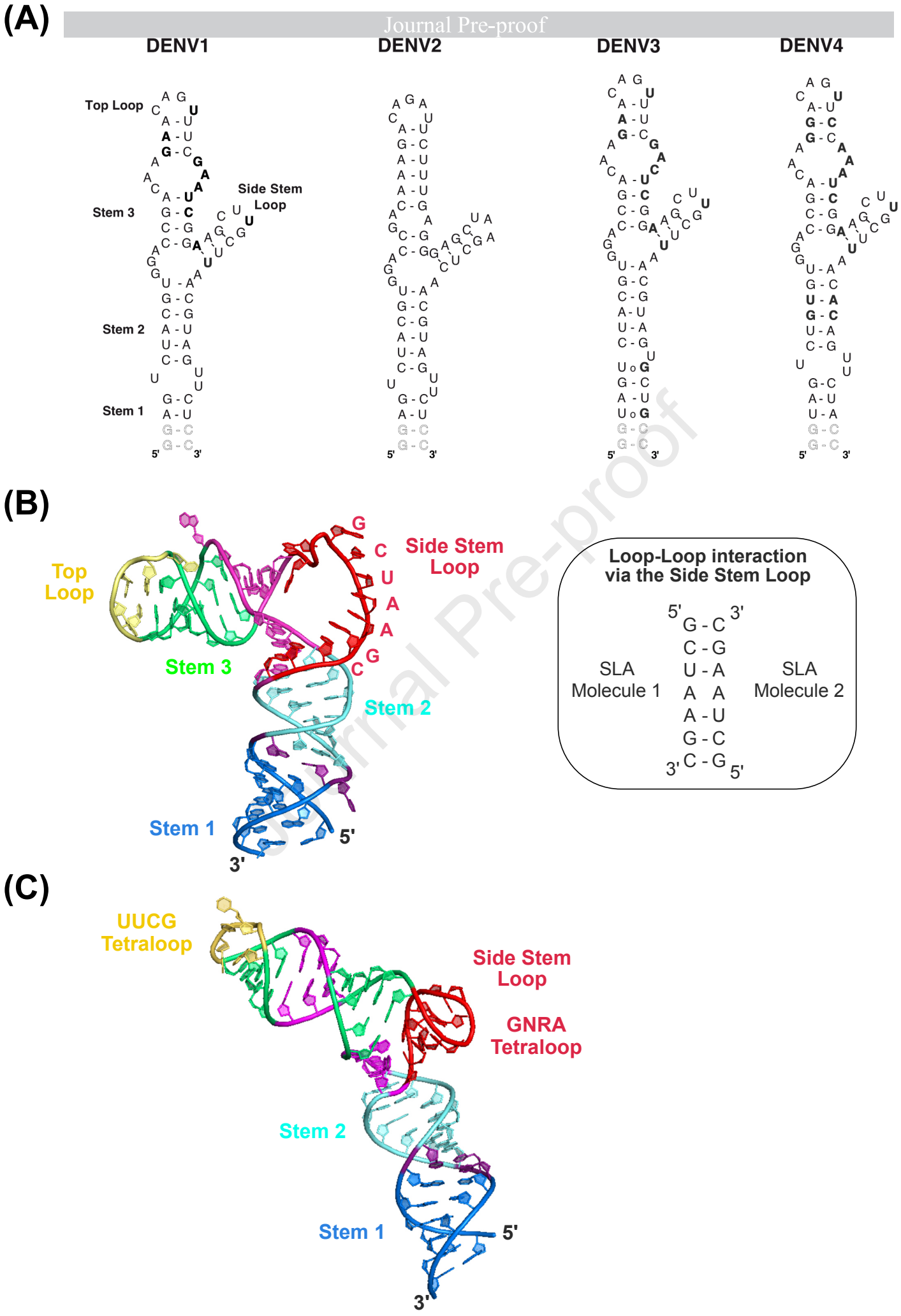

Figure 1

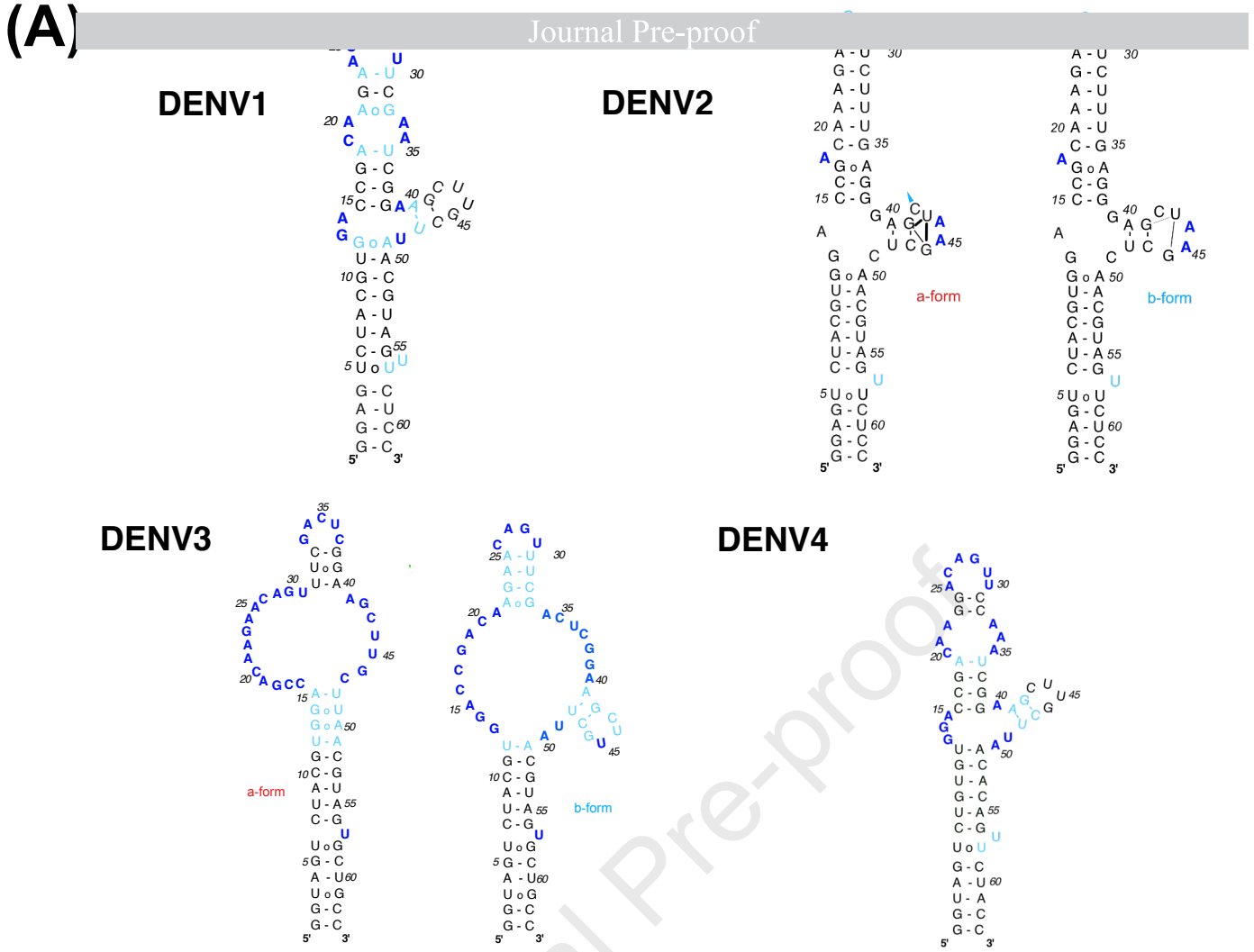

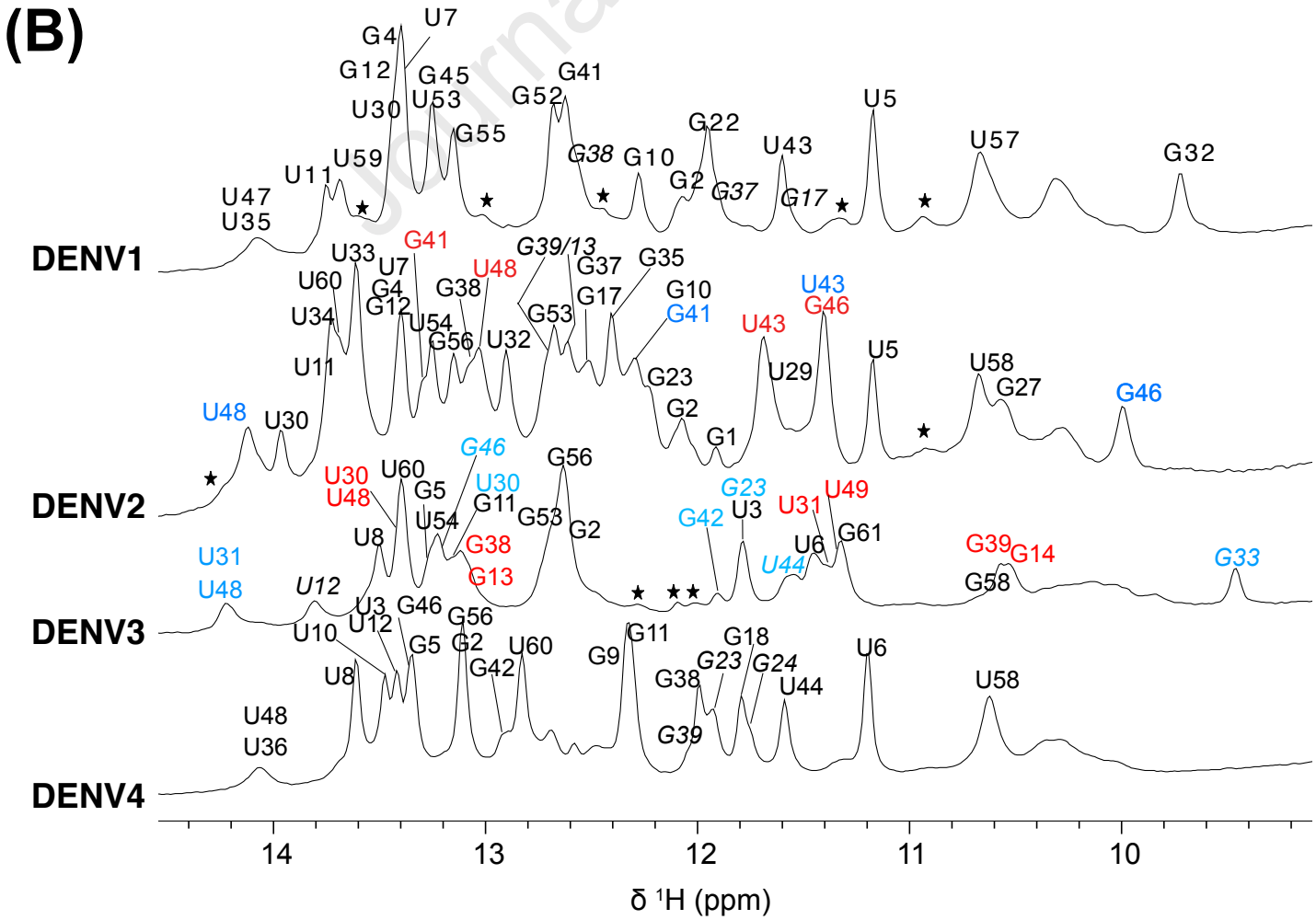

Figure 2

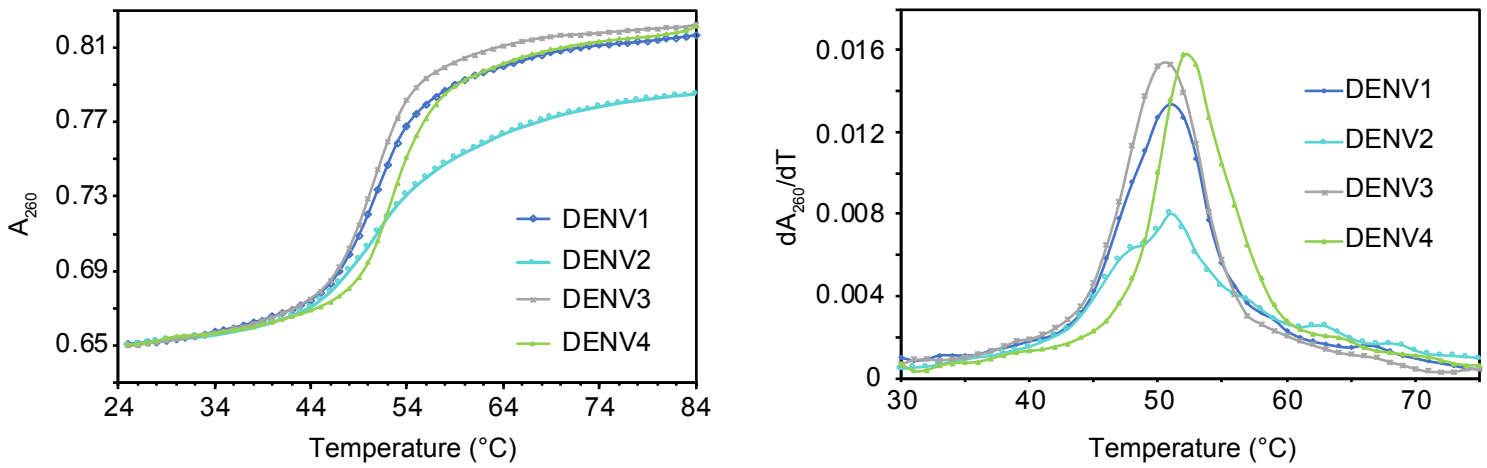

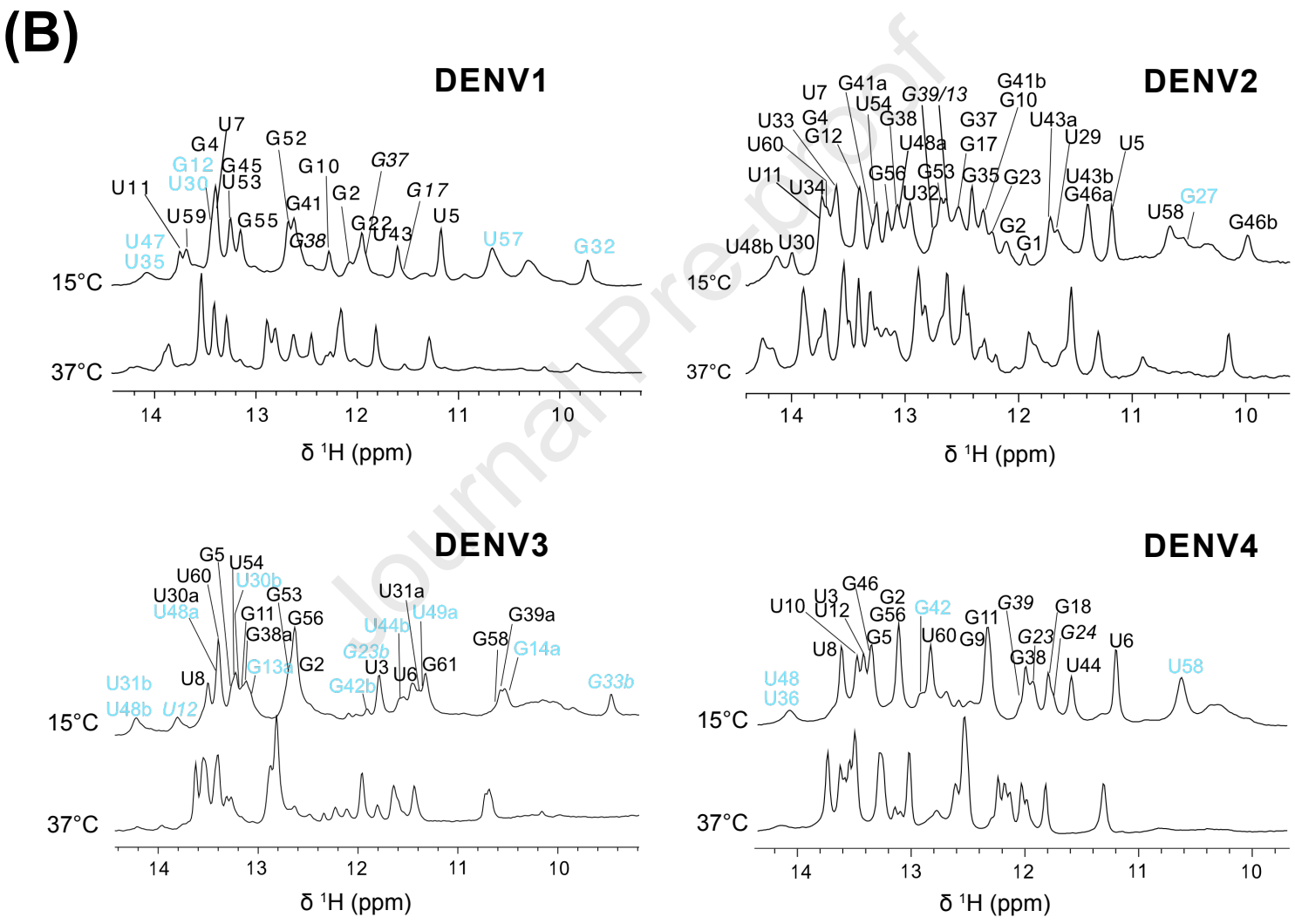

Figure 3

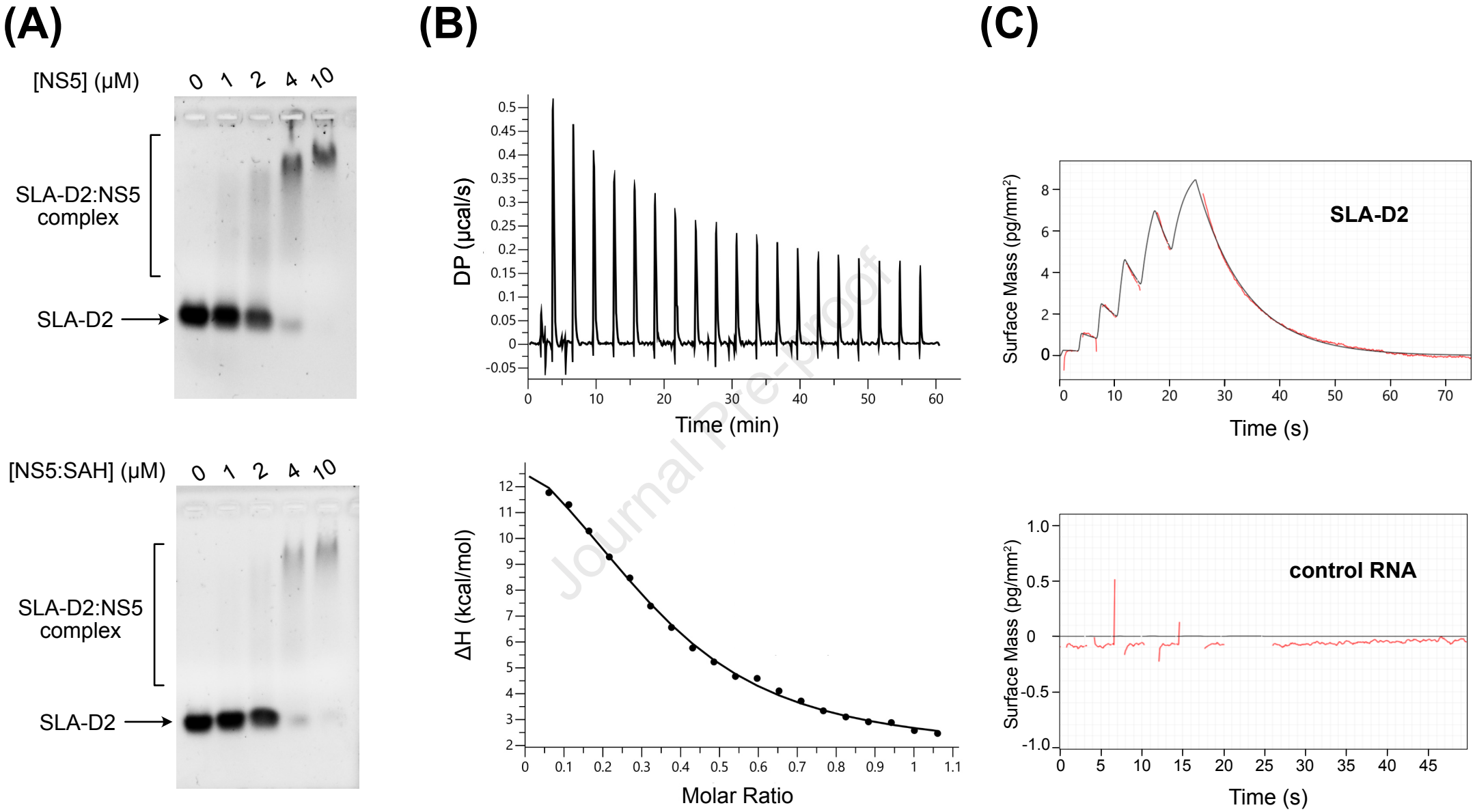

Figure 4

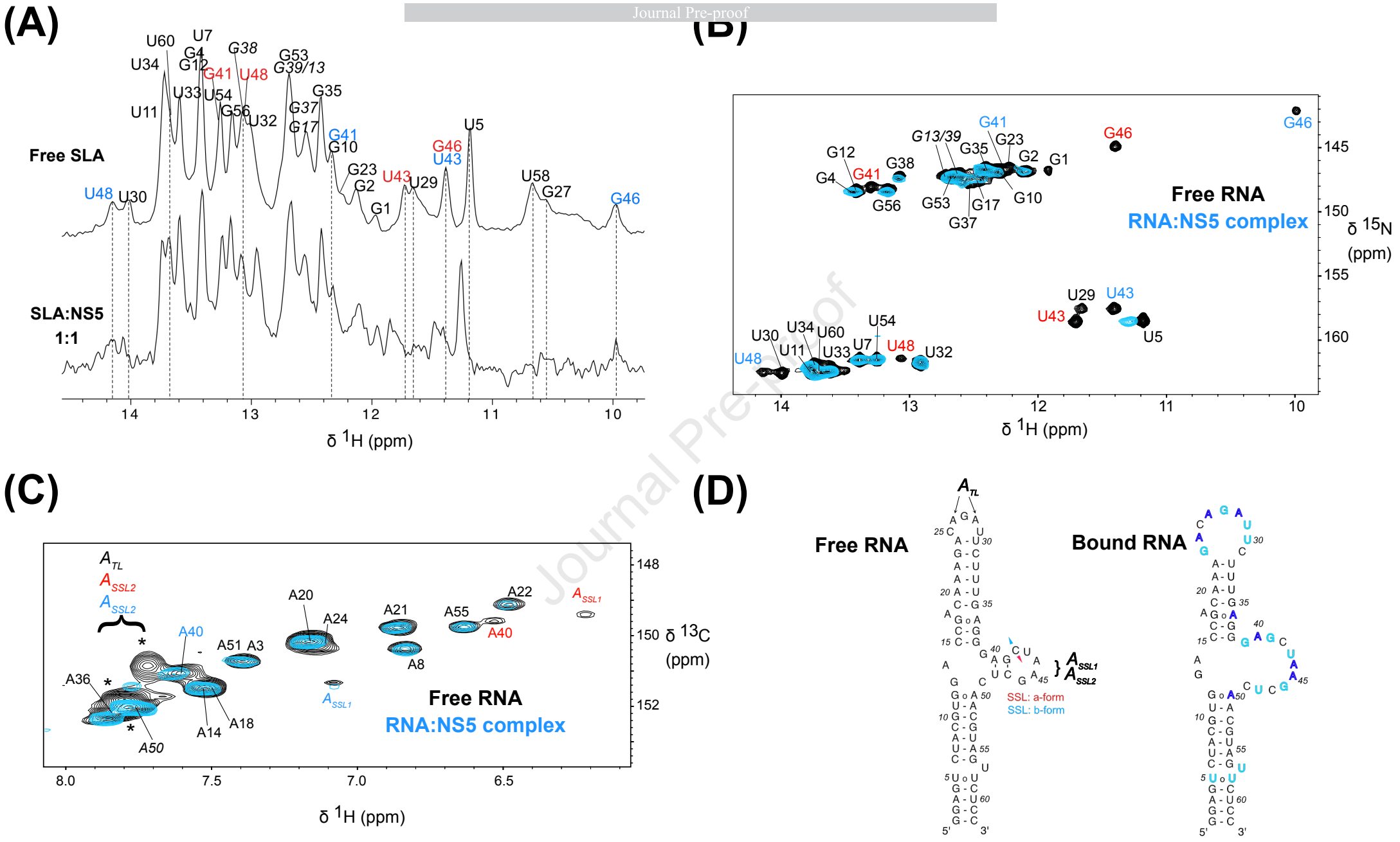

Figure 5

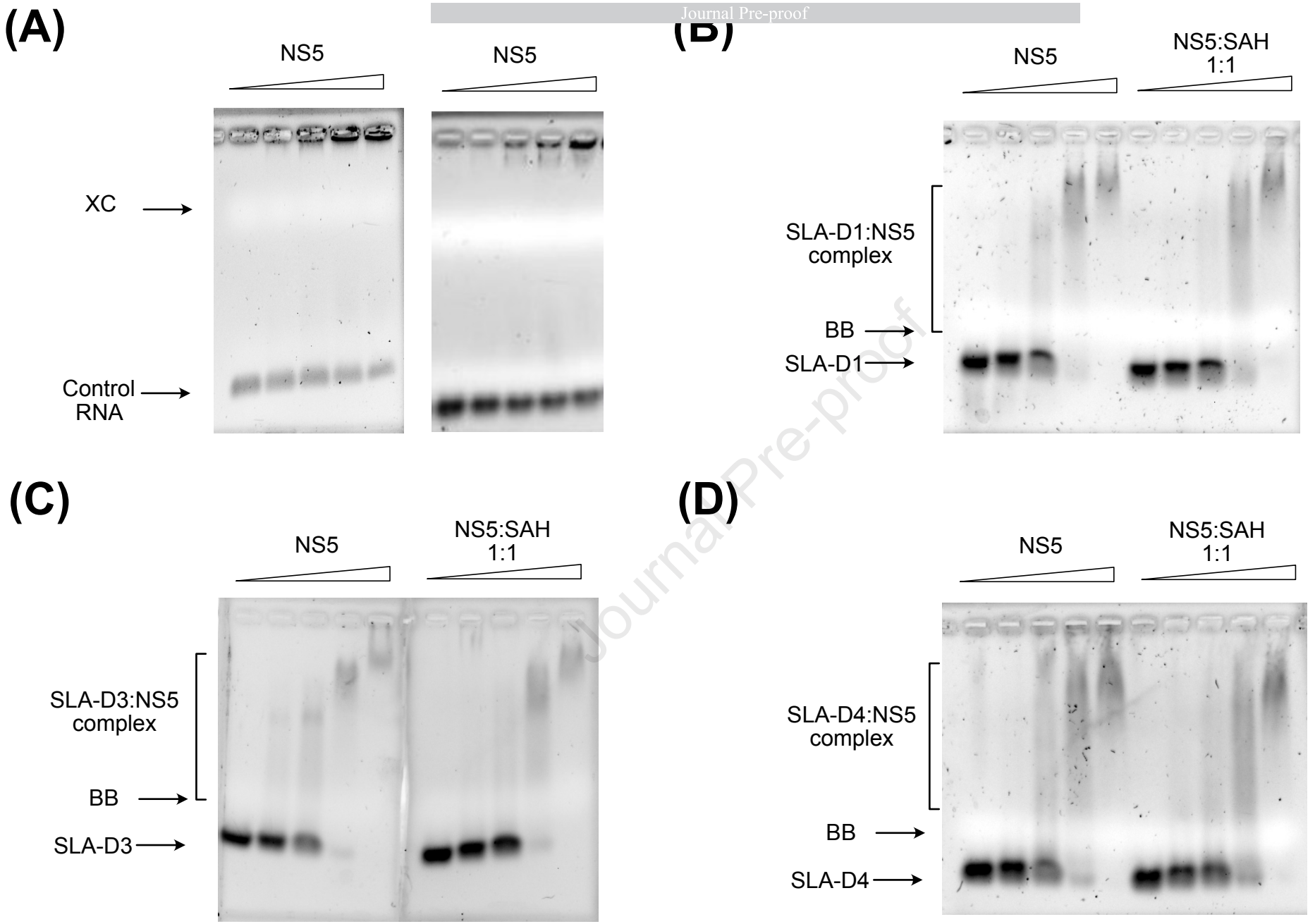

Figure 6

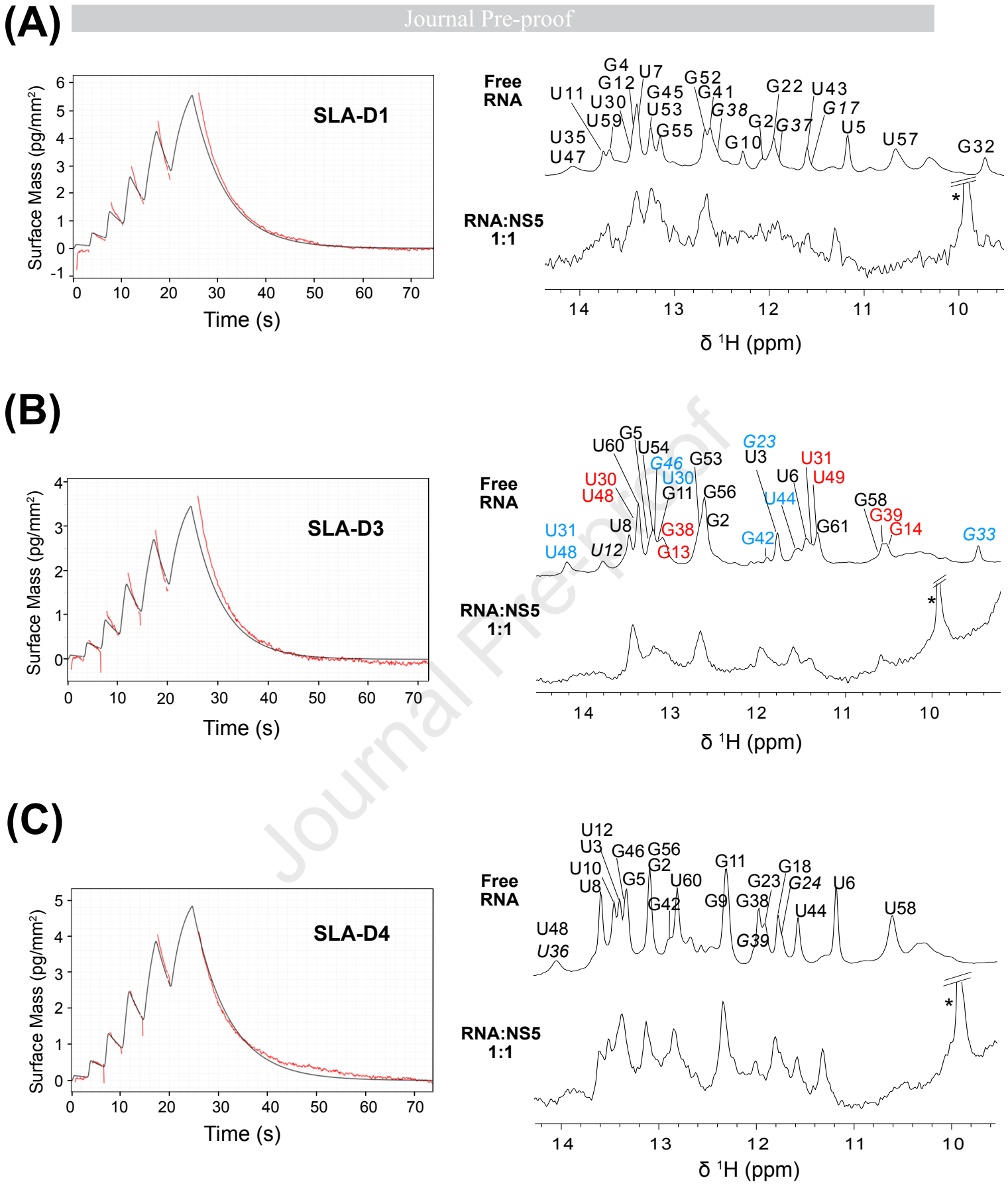

Figure 7

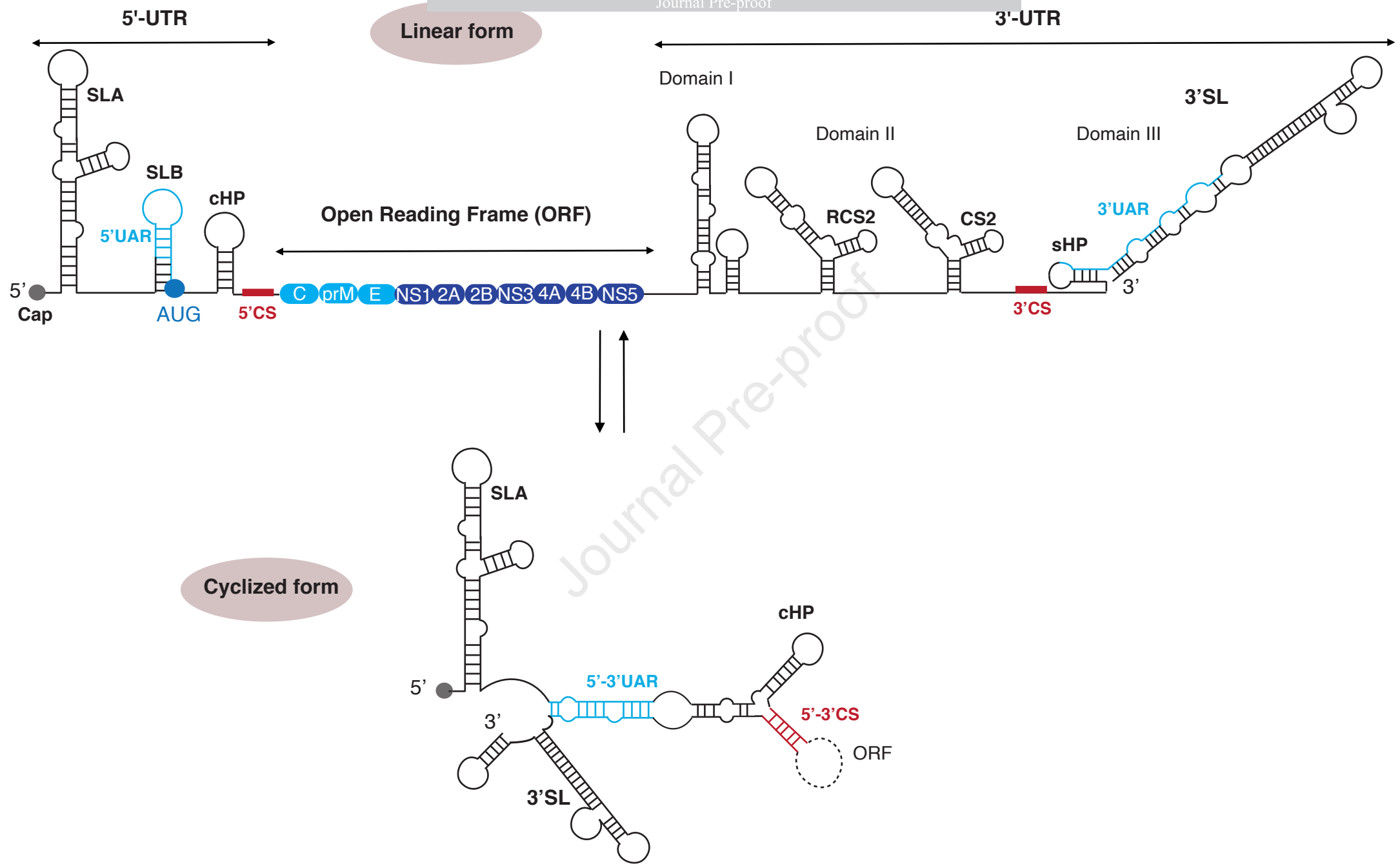

Figure 8

Highlights

- SLA RNA from DENV-1 to -4 exhibit structural and dynamics differences.
- First NMR description of viral NS5 polymerase binding to SLA RNA.
- Binding of NS5 to serotype-specific SLA induces structural rearrangement.
- Binding of NS5 to a non-serotype-specific SLA occurs through different mechanisms.

***BIOCHIMIE* conflict of interest declaration**

Title : Characterization of SLA RNA promoter from Dengue virus and its interaction with the viral non-structural NS5 protein

Authors: Karl Brillet[1], Marta Janczuk-Richter[2], Amanda Poon[2], Joanne Laukart-Bradley[2], Eric Ennifar[1] & Isabelle Lebars[1,*]

We have no conflict of interest to declare.